The proton size

Jean-Philippe Karr, Dominique Marchand, Eric Voutier

The proton size

Jean-Philippe Karr[1,2,*]**, Dominique Marchand**[3]**, and Eric Voutier**[3]

[1]Laboratoire Kastler Brossel, Sorbonne Université, CNRS, ENS-Université PSL, Collège de France, France
[2]Université d'Evry-Val d'Essonne, Université Paris Saclay, France
[3]Laboratoire de Physique des 2 Infinis Irène Joliot-Curie (IJCLAB), Université Paris Saclay, CNRS/IN2P3, France
[*]e-mail: karr@lkb.upmc.fr

ABSTRACT

The proton charge radius has been measured since the 1950s using elastic electron–proton scattering and ordinary hydrogen atomic spectroscopy. In 2010, a highly accurate measurement of the proton charge radius using, for the first time, muonic hydrogen spectroscopy unexpectedly led to controversy, as the value disagreed with the previously accepted one. Since then, atomic and nuclear physicists have been trying to understand this discrepancy by checking theories, questioning experimental methods and performing new experiments. Recently, two measurements from electron scattering and ordinary hydrogen spectroscopy were found to agree with results from muonic atom spectroscopy. Is the 'proton-radius puzzle' now resolved? In this Review, we scrutinize the experimental studies of the proton radius to gain insight on this issue. We provide a brief history of the proton before describing the techniques used to measure its radius and the current status of the field. We assess the precision and reliability of available experimental data, with particular focus on the most recent results. Finally, we discuss the forthcoming new generation of refined experiments and theoretical calculations that aim to definitely end the debate on the proton size.

Key points

- The charge radius of the proton can be determined using two different experimental techniques: measurements of electron–proton elastic scattering cross sections and high-resolution spectroscopy of the hydrogen atom.

- A decade ago, the precision of the atomic spectroscopy method was greatly improved using muonic hydrogen atoms, wherein the electron is replaced by a muon. However, the value of the proton radius was in disagreement with previous determinations, giving rise to the 'proton-radius puzzle'.

- The latest results from refined scattering and spectroscopy experiments agree with the muonic value. This questions the estimation of systematic uncertainties in previous scattering and ordinary hydrogen experiments.

- More measurements are needed to confirm or disprove this trend. Various projects are in progress, aiming to improve some aspects of existing techniques or using new approaches.

Website summary: The charge radius of the proton is controversial as measurements by different methods disagree. Recent results indicate that these measurements might be reconciled. In this Review, we discuss the experimental techniques used to measure the proton radius and describe the current status of the field as well as forthcoming experiments.

Introduction

Protons, neutrons and electrons are the building blocks of the visible matter that constitutes our surrounding world. The free neutron is an unstable particle that transforms into a proton within a mean time of 15 min. By contrast, the free proton, with a lifetime of more than 10^{34} years, has not been found to be experimentally unstable despite the suggestions of grand unified theories. Unlike the electron, which is a point-like elementary particle, the proton is an extended compound object with a size that can be characterized by a radius.

In 1911, Ernest Rutherford formulated his theory of the atomic nucleus[1] after observing the deflection of α particles from a thin gold foil. Rutherford subsequently discovered the proton in 1919 in a series of experiments studying the collision of α particles with light atoms[2]. The development of molecular beams enabled Otto Stern and collaborators to measure the proton magnetic moment in 1933 (refs[3,4]), which was found to be unexpectedly large, indicating that the proton was not an elementary particle. Although suspicion of an internal structure suggests a spatial size, experimental proof of proton extension was not obtained until 1955, when Robert Hofstadter observed that the elastic scattering of an electron beam by a hydrogen target

differed from expectations assuming a point-like proton[5]. By the end of the 1950s, there was substantial evidence of the peculiar nature of the proton but no real explanation of its origin.

The first step towards understanding the structure of the proton came in 1964, when Murray Gell-Mann[6] and George Zweig[7] independently proposed the quark model to explain the structure of hadrons. Experimental evidence supporting this sub-structure was obtained in 1969 by Martin Breidenbach and collaborators (ref.[8]), with the observation that the inelastic interaction of electrons with protons becomes independent of the transferred energy at high excitation energies. Quantum chromodynamics (QCD) subsequently developed as the, now well-established, theory of the strong interaction between partons (that is, quarks and gluons). Nevertheless, understanding the global properties of the proton from QCD first principles remains a challenging task.

After a century of scientific research, the proton is still mysterious in many ways. The parton model describes a fast-moving nucleon as a collection of quasi-free quarks, antiquarks and gluons. But, how does the proton mass emerge from almost massless constituents? And, how is the quantum spin 1/2 of the proton built from such an assembly? The theoretical framework of generalized parton distributions [9–11] offers a universal parameterization of the parton structure to apprehend these issues, including the effects of structure on the proton size. New techniques involving polarized electron beams or targets have been demonstrated[12, 13] in which, analogous to X-ray crystallography, the light produced by electrons is scattered by the partons to reveal the details of the internal structure of the proton. The combination of these experimental tools with new accelerator facilities, such as the future electron–ion collider, is expected to provide answers to these fundamental questions.

In this context, it may appear anachronistic that, over the past decade, the scientific community is still debating the precise value of a macroscopic quantity such as the proton charge radius. The precision of experimental methods, made possible by technological advances, is undoubtedly the principal factor generating this discussion. Two techniques have been developed to experimentally determine the proton charge radius: the subatomic physics method based on the elastic scattering of electrons off protons (e–p), which is a continuation of the original experiment performed by Hofstadter in 1955 (ref.[5]), and the atomic physics method, which relies on hydrogen spectroscopy. Numerous measurements have been performed using both techniques, providing a wealth of values that were gathered by the Committee on Data for Science and Technology (CODATA) in 2006 to give a value of 0.8760(78) fm for the atomic physics method[14] and a value of 0.895(18) fm for the subatomic physics method[15]. In 2010, the A1 Collaboration at the Mainzer Mikrotron (MAMI, Germany) extensively measured the e–p cross section and obtained a value of 0.879(8) fm (ref.[16]), which is so far the most precise value for this technique and in agreement with previous e–p scattering and hydrogen spectroscopy determinations. Simultaneously, the CREMA (Charge Radius Experiments with Muonic Atoms) Collaboration at the Paul Scherrer Institute (PSI, Switzerland) performed a challenging muonic hydrogen spectroscopy experiment and reported a much more accurate value of 0.84184(67) fm (ref.[17]), in disagreement with previous results obtained with both atomic and subatomic methods. This CREMA value was later supported by two other muonic spectroscopy results on hydrogen[18] and deuterium[19]. The proton seen by muons thus appeared significantly smaller than that seen by electrons.

The CREMA results challenged the certainties of the scientific community, and substantial efforts were devoted to searching for solutions to this so-called proton-radius puzzle (see earlier reviews[20–23]). A tantalizing possibility is that this discrepancy reveals violation of lepton universality, that is, a fundamental difference between electron–proton and muon–proton interactions caused by a new force beyond the Standard Model. However, as none of these studies successfully resolved the discrepancy, it gradually became clear that further insight could only come from new experiments. Two results from hydrogen spectroscopy, in 2017 (ref.[24]) and 2018 (ref.[25]), further confused the situation, as one result agreed with the smaller (muonic) radius and the other with the larger (electronic) one. In 2019, an additional hydrogen spectroscopy value of 0.833(10) fm (ref.[26]) and an e–p scattering result of 0.831(14) fm (ref.[27]) were released, both supporting the smaller radius.

Is the proton-radius puzzle solved? Rather than trying to give a definitive answer, this Review aims to summarize the present state of knowledge on this matter. After describing the different experimental methods, we present and assess the available data, focusing on the most recent results. Finally, we offer our perspective on future measurements that could conclusively settle the discord, either by refining existing techniques or using new approaches.

Electron elastic scattering

The e–p elastic process corresponds to the scattering of an electron by a proton, with the latter remaining intact after the interaction. The observed angular distributions of the scattered electron and the recoil proton result from their electromagnetic interaction. In a quantum electrodynamics (QED) first-order picture, namely the Born approximation, the electromagnetic interaction is modelled by the exchange of a virtual photon with a squared four-momentum transfer q^2, that is, a particle with quantum photon characteristics that exists temporarily for a period of time determined by the time–energy uncertainty principle. The number of particles scattered at a given angle depends on the strength of the proton electromagnetic field generated by the charge and magnetization distributions inside the proton. Electron scattering accesses these distributions through the momentum-dependent electric ($G_E \equiv G_E(Q^2)$) and magnetic ($G_M \equiv G_M(Q^2)$) form factors, where $Q^2 = -q^2$ by convention as

q^2 is negative in the considered kinematical domain. These form factors parameterize the interaction and can be interpreted, in a non-relativistic approach, as the Fourier conjugates of the spatial charge and magnetization densities, respectively. The charge radius of the proton, r_p, is defined from the derivative of the electric form factor with respect to Q^2:

$$r_p = \sqrt{-6 \left. \frac{dG_E(Q^2)}{dQ^2} \right|_{Q^2=0}}. \tag{1}$$

Thus, electron scattering experiments access r_p through the slope of the electric form factor at $Q^2=0$.

Measurements of the electromagnetic form factors of the proton have been carried out for decades at numerous electron accelerator facilities using different experimental techniques (Box 1). The measured e–p cross section is a linear combination of the squared electric and magnetic form factors, from which G_E^2 and G_M^2 can be isolated by taking advantage of the sensitivity of the cross section to the beam energy and scattering angle. At large squared four-momentum transfer ($Q^2 \gg m_p^2$ where m_p is the proton mass), polarization experiments[29] were shown to be more reliable than those relying on this so-called Rosenbluth separation technique[28]. In polarization experiments, the transfer of the longitudinal polarization of an electron beam to the interacting proton in the elastic process[30–32], or the cross-section asymmetry of the elastic interaction of a longitudinally polarized electron beam with a polarized proton target[33], is used to measure the ratio G_E/G_M. The discrepancies between the cross-section and polarization methods (Box 1) are still under investigation. In particular, it has been proposed that higher orders to the Born approximation of the electromagnetic interaction — that is, the exchange of more than one virtual photon — should be considered[34, 35]. Such mechanisms may reconcile these two techniques, but experimental investigations[36–38] have not yet indisputably confirmed this hypothesis. These effects are predicted to have a small impact on the determination of the proton charge radius[39], but their theoretical evaluation remains model-dependent[40].

The proton charge radius, r_p, defined by Eq. (1) is also commonly interpreted non-relativistically as the square root of the average value of r^2 in a spherically symmetric charge density. However, it must be stressed that this picture is not relativistically supported[41]. The relationship between r_p and $\sqrt{\langle r^2 \rangle}$ is derived theoretically from the moment expansion of the Fourier representation of the form factors. In this respect, two essential difficulties arise when considering the interpretation of the e–p elastic process. Because the initial and final protons differ in momentum, e–p scattering does not access a probability density in the quantum sense of the square of a wave function. Furthermore, as the proton is a composite object formed of highly relativistic constituents, a non-relativistic interpretation of form factors may appear limited. The light-cone formalism offers an approach to evaluate these relativistic effects from generalized parton distributions, which can be obtained experimentally or through lattice QCD calculations. A sizeable difference of 0.02 fm^2 between the relativistic and non-relativistic values of $\langle r^2 \rangle$ has been reported[41], which is significant on the scale of the discrepancy in the proton-radius puzzle. However, in the absence of an extended experimental database and sufficiently accurate lattice calculations of generalized parton distributions, it is not yet possible to use this approach to extract the proton charge radius.

Box 1| Measuring the electromagnetic form factors of the proton

The probability of finding an electron at the spherical angles (θ, ϕ) after interacting elastically with a proton is described by the differential electron–proton (e–p) cross section (σ_{ep}), which can be written in the one-photon exchange Born approximation and considering ultra-relativistic electrons as

$$\frac{d^2\sigma_{ep}}{d\theta d\phi} = \frac{d^2\sigma_{Mott}}{d\theta d\phi} \frac{E'}{E} \frac{\varepsilon G_E^2 + \tau G_M^2}{\varepsilon(1+\tau)}$$

where the Mott cross section (σ_{Mott}) is the interaction probability of an electron within the Coulomb field generated by a static point-like spin-1/2 proton, the ratio of the scattered (E') and incoming (E) electron energies takes into account the proton recoil, and the last term is the proton-size effect described by the Q^2-dependent electric (G_E) and magnetic (G_M) form factors. $\tau = Q^2/4m_p^2$ is a kinematical factor defined by the squared four-momentum transfer $Q^2 = 2m_p(E - E')$ and the proton mass (m_p). ε is the polarization of the virtual photon defined by

$$\varepsilon = \left(1 + 2(1+\tau)\tan^2(\theta/2)\right)^{-1}.$$

The Rosenbluth separation technique takes advantage of the ε-dependence of the structure term to extract G_E^2 and G_M^2 from cross-section measurements at different ε and constant Q^2 by varying the electron beam energy and the scattering angle.

Polarization observables provide another approach to measuring the proton form factors. In the elastic interaction of a longitudinally polarized electron beam (P_e), the proton gains a polarization that can be decomposed into longitudinal (P_l) and transverse (P_t) components with respect to the direction of the virtual photon. The measurement of these components provides direct access to the ratio of G_E to G_M following the expression

$$\frac{G_E}{G_M} = -\frac{P_t}{P_l} \frac{E + E'}{2m_p} \tan(\theta/2).$$

Considering instead a proton polarized in the reaction plane formed by the incoming and scattered electrons and perpendicular to the virtual photon direction, the cross-section asymmetry $A = hP_e P_\perp A_\perp$ measured upon reversal of the beam helicity (h) or the orientation of the proton target polarization ($P_\perp$), with

$$A_\perp = -2\sqrt{\tau(1+\tau)} \frac{(G_E/G_M)\tan(\theta/2)}{(G_E/G_M)^2 + (\tau/\varepsilon)},$$

provides another method for obtaining the form factor ratio. The polarization technique was initially developed to circumvent the difficulty in accurately measuring G_E at large Q^2, which is due to its reduced contribution to the cross section compared with G_M.

The figure shows plots of the ratio of the electromagnetic form factors obtained through the Rosenbluth separation (panel **a**) and polarization (panel **b**) techniques. Comparison of the plots reveals large differences between the values obtained using these methods, which have not yet been indisputably resolved. The data points are labelled by the first author and year; the data set from ref.[56] is restricted to the Rosenbluth subset. The dashed line indicates the empirical scaling observation $G_M = \mu G_E$ from early scattering experiments.

Data for panel **a** from refs[42–56]. Data for panel **b** from refs[57–71].
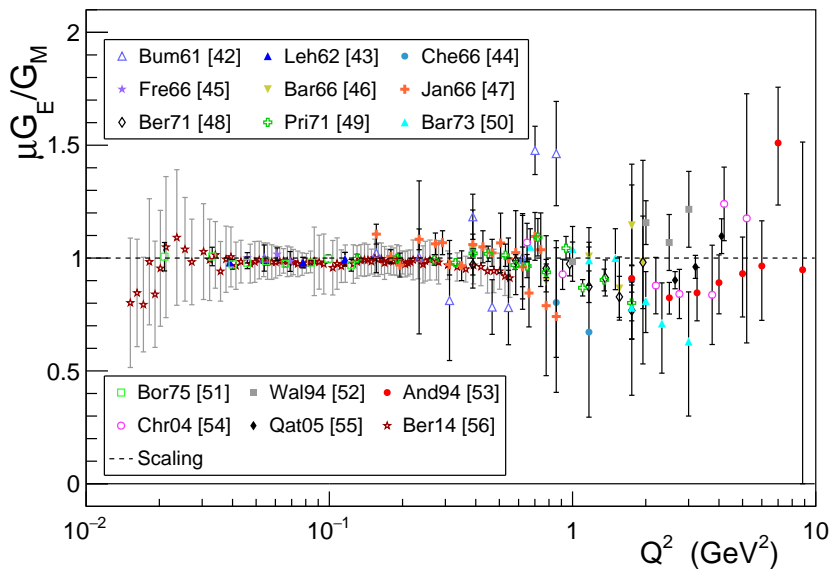
a
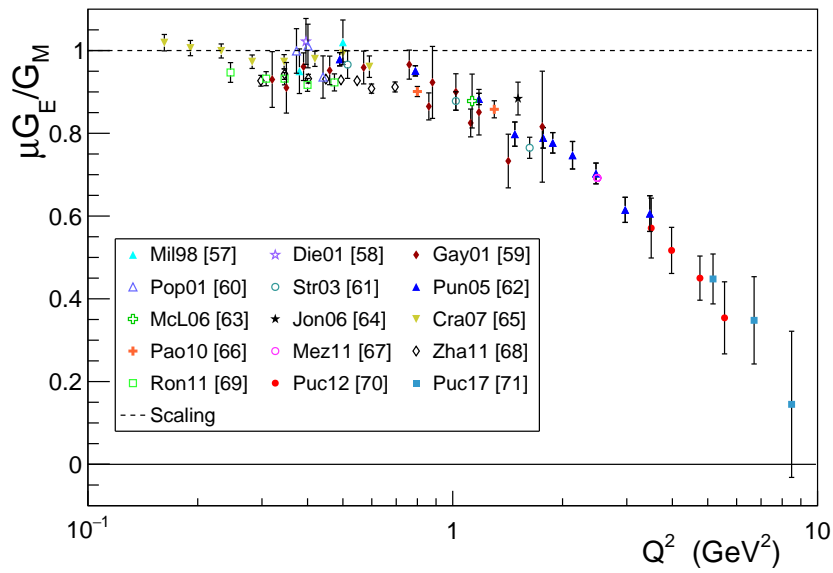
b

Atomic spectroscopy

The proton charge radius, as defined by Eq. (1)[41], can also be deduced from the shift it produces in the energy levels of the hydrogen atom[72]. This effect has a simple physical origin: S-state electrons spend some time inside the proton charge cloud, where they experience a Coulomb attraction that is weaker than that of a point-like charge, shifting the energy levels upwards. This finite-size shift represents only a small contribution to the QED shift of energy levels that was first evidenced by measuring the energy separation between the $2S_{1/2}$ and $2P_{1/2}$ states, known as the Lamb shift[73]. Bound-state QED corrections[74] thus need to be calculated accurately to extract the finite-size contribution from the comparison of experimental and theoretical transition frequencies. Many precise spectroscopic measurements have been performed in ordinary hydrogen over the past four decades, whereas the first experiment in muonic hydrogen[17] took place in 2009, leading to the so-called proton-radius puzzle.

In ordinary hydrogen, the approximate dependence of the energy of an atomic level $E_{n,l}$ (where n and l are the principal and angular momentum quantum numbers, respectively) on the proton radius is given by

$$E_{n,l} \simeq -\frac{R_\infty}{n^2} + \delta_{l,0}\frac{L_{1S} + a\,r_p^2}{n^3} \qquad (2)$$

where $R_\infty \simeq 3.29 \times 10^6$ MHz is the Rydberg constant, $L_{1S} \simeq 8.172$ MHz is the Lamb shift of the 1S ground state for a point-like nucleus, and $a \simeq 1.56$ MHz fm^{-2}. The finite-size shift (last term of Eq. (2)) is very small as the proton is five orders of magnitude smaller than the Bohr radius and represents 0.014% of the $2S_{1/2}$–$2P_{1/2}$ Lamb shift or a fractional shift of a few 10^{-10} for optical transitions (Fig. 1). Nevertheless, the very high precision achieved both in spectroscopic measurements and in theoretical calculations of transition frequencies allows the proton radius to be extracted with a sub-percent relative uncertainty[75]. As energy levels depend on R_∞ and r_p in Eq. (2), two measurements are needed to simultaneously determine these two constants. In this regard, the 1S–2S transition has a key role, as it is the only narrow transition and has been measured with a record precision of a few 10^{-15} (ref.[76,77]). All other transitions have much larger natural widths and cannot be measured as precisely. Each of these transitions can be combined with the 1S–2S measurement to extract R_∞ and r_p. Experiments are performed with room-temperature or cryogenic atomic beams and transitions detected either by collecting the fluorescence from the excited state or, if the metastable 2S state is involved, by measuring a signal proportional to the remaining population in that state.
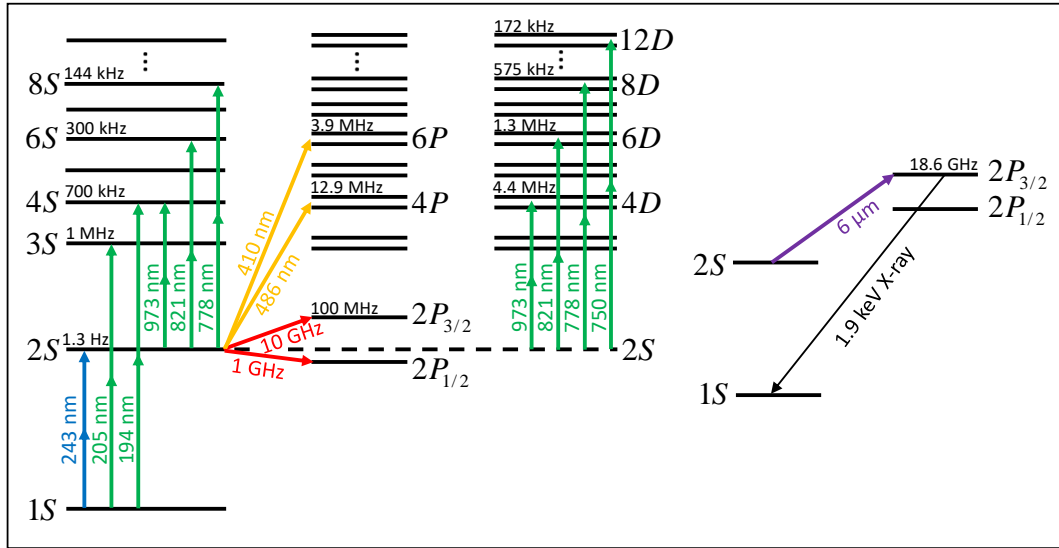
Figure 1. Transitions in electronic and muonic hydrogen. Spectra showing the transitions in electronic (left) and muonic (right) hydrogen. The spectra are not to scale, and the hyperfine structure is not shown. For electronic hydrogen, the arrows indicate all transitions that contribute to the determination of the proton charge radius and a few that are being considered for new measurements. The blue arrow is the very precisely measured 1S–2S transition, which has a pivotal role in the joint determination of the Rydberg constant and the proton charge radius. The yellow and green arrows denote one-photon and Doppler-free two-photon optical transitions, respectively, while the red arrows correspond to microwave transitions. In muonic hydrogen, the purple and black arrows are, respectively, the measured 2S–2P transition and the X-ray Lyman-α transition, by which its excitation is detected. The natural widths of the levels are given in frequency units, and the transition wavelengths (or frequencies for the 2S–2P transitions) are indicated.

In muonic hydrogen, a proton is orbited by a negative muon, which has a mass larger than the electron mass, leading to a Bohr orbit that is 200 times smaller. This increases the overlap of the wave function with the proton and, hence, the S-state energy levels are a few million times more sensitive to the nuclear size and structure. For muonic hydrogen, the finite-size effect on the 2S–2P Lamb shift is as large as 2%[78]:

$$\Delta E_{2S-2P} = 206.0808(61) \text{ meV} - 5.2272 \, r_p^2 \text{ meV fm}^{-2}. \tag{3}$$

This explains how a moderately precise (~ 10 ppm) measurement in muonic hydrogen led to a tenfold improvement in the r_p value[17,18]. Note that the calculation of finite-size effects is considerably more involved than in ordinary hydrogen, because the contribution from higher-order moments of the nuclear charge distribution and from the proton polarizability must be taken into account to obtain sufficient accuracy.

The challenges of producing and manipulating exotic atoms sets the muonic hydrogen experiment apart from ordinary hydrogen spectroscopy. The experiment was performed using the world's most intense muon beam at PSI. Ultralow-energy (2 keV) negative muons (μ^-) are stopped in a low-density hydrogen gas. The muons slow down in ionizing collisions, eventually replacing an electron in an H_2 molecule, which breaks up and leaves a highly excited μp atom. Radiative and collisional processes induce de-excitation, leaving $\sim 1\%$ of all muons in the metastable 2S state. Triggered by the detection of an incoming muon, a laser pulse at a wavelength of 6 μm illuminates the muon stop volume. The transition signal is obtained by detecting the 2P→1S Lyman-α photons at 1.9 keV emitted after a successful laser-induced 2S→2P transition (Fig. 1). With 300 μ^- detected per second in the muon entrance detectors, a signal rate at the peak of the resonance of about six detected X-rays per hour was achieved after offline cuts. The measurement was possible owing to the small background rate of one event per hour. Several hundred laser-induced events were detected per resonance, leading to a statistical uncertainty of a few percent of the width, that is, ~ 1 GHz.

Assessment of existing data

Numerous values of the proton radius have been extracted from electron scattering and hydrogen spectroscopy measurements and are presented chronologically in Fig. 2 and Fig. 3, respectively. In the following, we discuss the precision of each experimental method in order to assess the significance of the observed discrepancies and the likelihood of different solutions.

Experimental errors in the muonic hydrogen measurement[17,18] can be ruled out. From the purely spectroscopic point of view, this is not a very high-precision measurement as it is limited by the low statistics inherent to experiments with muons. The only relevant systematic uncertainty (300 MHz) stems from the laser frequency calibration, and is due to the relatively large laser bandwidth (~ 1.8 GHz). Note that a 1 GHz frequency shift changes the inferred value of r_p by only 0.00047 fm. All other systematic effects typical of laser spectroscopy, such as AC and DC Stark shifts, as well as Zeeman, Doppler and collisional effects, are much smaller. Indeed, the close proximity of the muon and proton results in huge internal fields that are hardly affected by small external perturbations. On the theoretical side, the QED calculations used to extract r_p have been checked and further developed [74,79–87]. A debate arose about the magnitude of the proton polarizability correction in the two-photon-exchange diagram[88] but was settled after several calculations showed satisfactory agreement[78,89,90]. Consequently, the muonic proton radius is now a well-established experimental result and no longer questionable.
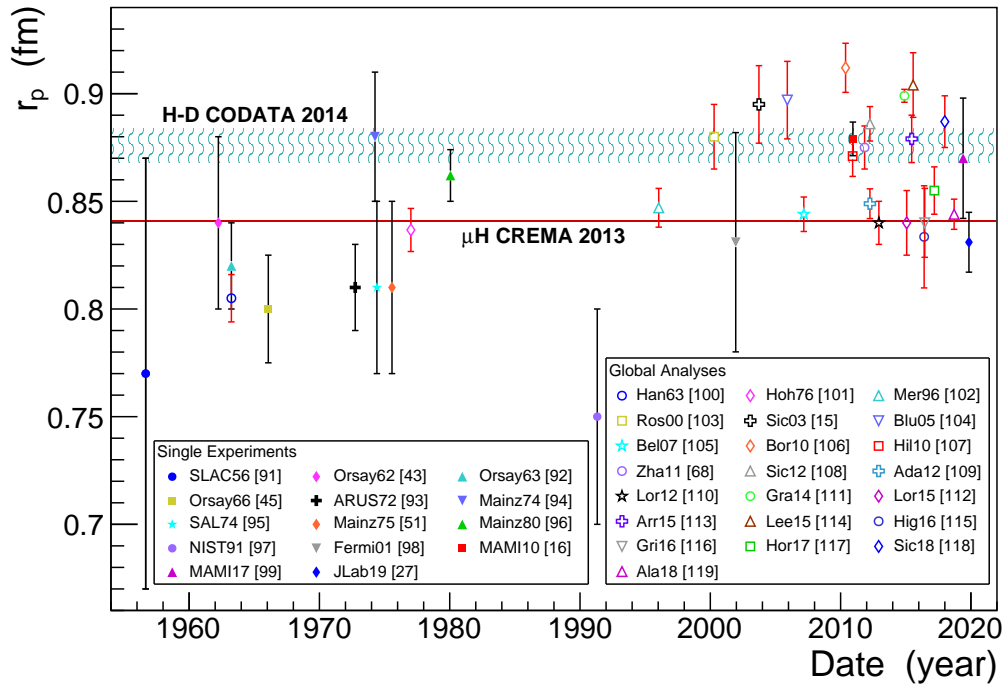
Precision of scattering experiments

Comparison of results from single scattering experiments and from global analyses of data sets reveals that the precision of the scattering technique improved from the very first measurement at SLAC in 1956 (ref.[91]) to culminate in the 2010 measurement at MAMI[16] (Fig. 2). Successive experimental and theoretical analyses also improved in their content and accuracy but differ from each other, in some cases, significantly. For instance, the increase in r_p from 0.862 fm (ref.[96]) up to 0.895 fm (ref.[15]) is due to Coulomb distortion effects and the refinement of fitting methods. The discrepancies between post-2010 analyses suggest the possibility of biases or a lack of consistency in the data set and cast doubt on the analysis methods. This situation makes it difficult to draw conclusions about the value of the proton radius from scattering measurements compared with the value from muonic atom spectroscopy. Nevertheless, two important observations are that the 2010 MAMI[16] measurement differs from the 2013 CREMA value[18] by 4.9 standard deviations (σ), and that the recent result from the proton radius experiment (PRad) at the Thomas Jefferson National Accelerator Facility (JLab, USA)[27], which supports the smaller CREMA value, differs from the 2010 MAMI value by only 3σ.

The scattering technique requires the slope of a function to be determined at a point that is experimentally inaccessible ($Q^2 = 0$), raising questions regarding the experimental determination of this function and the extrapolation procedure down to $Q^2 = 0$. This procedure requires accurate measurements of cross sections with excellent point-to-point normalization, which is a demanding task when aiming for high accuracy.

The major sources of systematic errors in these experiments originate from the relative normalization of experimental data, which involves the detection efficiency, the target purity, the experimental luminosity and radiative corrections. All scattering

Figure 2. Proton radius values from electron scattering experiments. Chronological overview of the values of the proton charge radius (r_p) determined from electron scattering measurements. The full symbols represent results from single experiments, labelled by their location and year. The open symbols are results of global analyses of the full or a part of the global elastic electron–photon scattering data set, labelled by the first author and year. The wide, blue band represents the CODATA 2014 recommended value obtained from hydrogen and deuterium (H–D) spectroscopy[75], and the thin, red band corresponds to the best estimate of the CREMA Collaboration[18] using muonic hydrogen (μH) spectroscopy. The error bars represent one standard deviation. Data for single measurements from refs[16,27,43,45,51,91–99]. Data for global analyses from refs[15,68,100–119].

experiments, except PRad, operated with magnetic spectrometers that select either the scattered electron and/or the recoil proton from solid CH_n or liquid hydrogen targets. The kinematic energy–angle correlation and the back-tracking of detected particles to the interaction region distinguish the elastic scattering from background processes, particularly those originating from the beam entrance and exit windows of the target cell. The luminosity, which corresponds to the product of the beam intensity with the target density, is monitored with an additional detector at a fixed location. The additional fixed detector provides a relative normalization link for identical kinematic settings (same Q^2 value) when the beam energy or the scattering angle is varied. Luminosity monitoring and the point-to-point normalization are particularly important for spectrometer experiments that cover a wide Q^2 range as angular scans are required at several fixed beam energies to separate the electric and magnetic form factors. Today, normalization systematics can be controlled at the sub-percent level; for example, the A1 Collaboration reported a value of 0.1%[56]. However, not all scattering experiments have been conducted under these strict controls, introducing further difficulties when combining different data sets. Owing to their model dependency, radiative corrections remain the main source of systematic uncertainties. Several prescriptions for addressing this issue at the leading order and beyond have been proposed, resulting in discrepancies of 0.5–1% (see ref.[131] for further discussion). The common practice of using a floating normalization factor when fitting experimental data usually absorbs these normalization systematics. However, when complex regressions are involved, as in the analysis of the 2010 MAMI data, this procedure may dramatically affect the final results[132].

The extrapolation of an experimental trend is in some way a guess on a more or less constrained behaviour. A given mathematical function can be an excellent interpolation of experimental data but a poor extrapolation. Determining the proton radius is an even more difficult problem as it concerns the slope and not the value of the function. Ideally, with very accurate data, the extrapolation of an interpolated function to zero is a well-constrained method. However, the extrapolation of real experimental data inevitably suffers from limitations, leaving room for systematic effects that are difficult to control when combining multiple data sets. The technique developed for the analysis of the 2010 MAMI data[56] has been scrutinized to

reveal possible flaws related to the sensitivity of the extrapolation to the functional form and to the upper limit of the Q^2 region considered for the interpolation[107,114,133]. For instance, a 1σ-compatibility with the CREMA result can be obtained by varying the Q^2 upper bound[115,116]. This restriction of the Q^2 interpolation region has been criticized[133,135–137]. Pseudo-data methods that mimic real experiments now provide a valuable handle on the systematics associated with these effects[56,133,134]. It is also worth noting that analyses based on theoretically motivated ansatzes[101,102,105,109,110,112,119] have consistently found a radius compatible with the CREMA result.

In terms of these systematic uncertainties, the recent PRad experiment[27] demonstrated major improvements and provided new insight into the proton-radius puzzle. Using an electromagnetic calorimeter, PRad simultaneously measured within the same detector the elastic e–p and the Møller e–e processes. This allowed for the measurement of a relative cross section with respect to an exactly calculable QED process, resulting in substantially reduced systematic effects associated with the detector efficiency and the luminosity. Additionally, unlike the spectrometer method, which requires different settings to perform Q^2 scans, the calorimeter technique allows for the simultaneous measurement of several Q^2 values with exactly the same experimental conditions — a major benefit for the control of point-to-point relative normalization effects. Furthermore, a windowless target made of a cryo-cooled hydrogen-gas flow was implemented, eliminating background and radiative contamination from target windows. Because of the very low Q^2 domain investigated, the elastic cross section at PRad is dominated by the electric form factor with no need for a Rosenbluth separation; this is very valuable for minimizing systematic effects. Using a non-magnetic detector and a relative cross-section measurement, radiative effects at PRad are different from those in spectrometer experiments but still represent the main source of cross-section systematics ($\sim 0.4\%$ on average). Relying on a refined extrapolation method[134] and exploring the smallest ever Q^2 domain, PRad is the first modern scattering experiment to agree with the muonic atom spectroscopy measurement but is not precise enough to statistically reject the 2010 MAMI result. The disagreement between the PRad and 2010 MAMI values is puzzling as it suggests incompatible form-factor data.
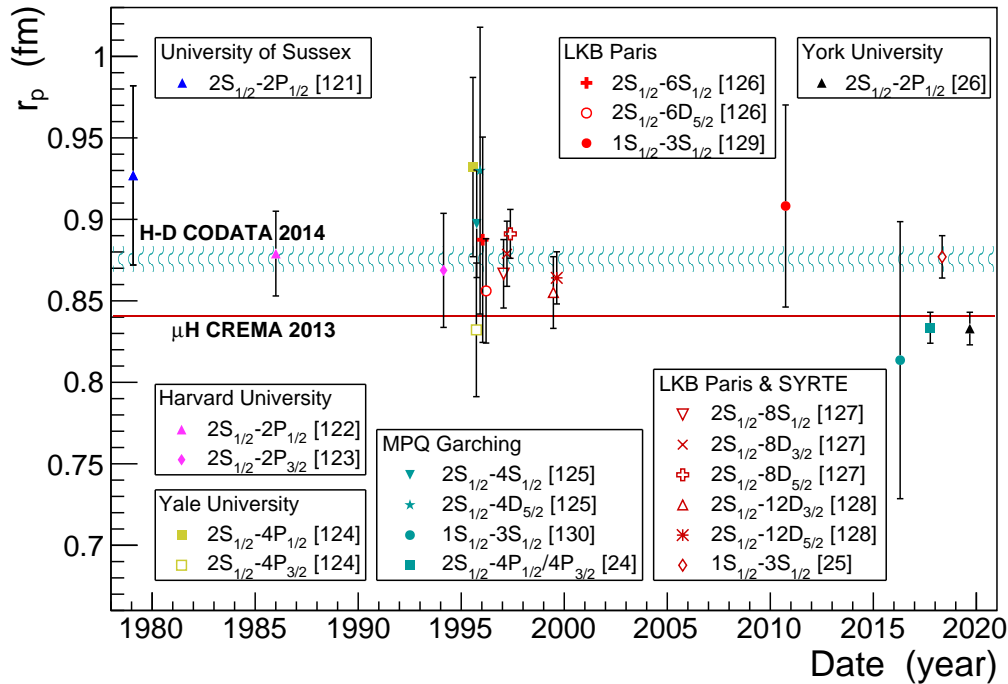
Precision of spectroscopy experiments

Ten different electronic transitions have been measured in electronic hydrogen (Fig. 1 and Fig. 3) with precisions in the 10^{-11}–10^{-12} range for optical transitions or 10^{-5}–10^{-6} for microwave ones. In Fig. 3, each measurement is combined with the 1S–2S measurement to extract r_{p} (note that the highly precise 1S–2S result is not needed for 2S–2P Lamb-shift measurements that have low sensitivity to the Rydberg constant and can be considered as pure measurements of the proton radius). Although almost all measurements favour a large proton radius, most of the results are compatible with the muonic hydrogen value within 1.5σ, and only two disagree by more than 2σ. The global least-squares adjustment performed by CODATA taking into account data prior to 2014 results in a 4σ discrepancy, or 4.5σ if deuterium measurements are also considered[75]. Calculations of the hydrogen atom Lamb shift (Eq. (2)) have steadily improved over several decades, with all relevant QED contributions having been evaluated independently by at least two different groups[74,75,138]. The theoretical uncertainty in the ground-state energy is currently estimated to be 1–2 kHz (refs[138–140]), which is much smaller than the ~ 100 kHz shift that would be required to cancel the discrepancy with the muonic hydrogen result.

High-resolution hydrogen spectroscopy experiments are challenging because of the relatively large natural widths of the measured lines (Fig. 1). Except for the 1S–2S line, the centre frequency should be determined to a small fraction (typically 10^{-3}–10^{-4}) of the natural width to achieve a sensitivity of a few percent to r_{p}. This requires high statistics, detailed understanding of the lineshape and careful evaluation of all systematic effects.

An important improvement in the 2S–4P measurement[24] was the atomic source. The group in Garching relied on a cryogenic beam and, instead of the previously used electron-impact technique, used Doppler-free two-photon laser excitation of the 1S–2S transition to produce atoms in a single Zeeman sublevel of the 2S states, leading to a simpler lineshape. The main systematic is the first-order Doppler effect, which, together with the 12.9 MHz natural width of the 4P state, is responsible for the 20 MHz linewidth. The Doppler shift is compensated by driving the transition with two precisely antiparallel beams, leading to opposite shifts. Furthermore, a previously unaccounted for quantum-interference effect in the fluorescence signal was evidenced and subsequently subtracted by observing its dependence on the laser polarization and the direction of emission. The obtained precision of 2.3 kHz ($\sim 10^{-4}$ of the linewidth) is an impressive achievement for this type of experiment.

A more powerful and stable laser source at 205 nm was implemented for the measurement of the 1S–3S Doppler-free two-photon transition[25,120], allowing for improved statistics and more detailed systematic studies. The experiment involved a room-temperature atomic beam, and the main systematic is the second-order Doppler shift. This shift is partially compensated by exploiting the motional electric field experienced by the atoms in a transverse magnetic field, which induces a Stark shift proportional to their squared velocity. In the data analysis, a two-parameter model of the velocity distribution in the atomic beam was used to compute the theoretical lineshape. Other notable systematics are the light shift and the pressure (collisional) shift, which are corrected by extrapolation to zero power and to zero pressure, respectively. The experimental uncertainty of 2.6 kHz ($\sim 2 \times 10^{-3}$ of the 1.35 MHz linewidth) is significantly reduced with respect to previous measurements[129,130].

Finally, the 2019 measurement of the $2S_{1/2}$–$2P_{1/2}$ Lamb shift by radiofrequency ($\nu \approx 1$ GHz) spectroscopy[26] has been

Figure 3. Proton radius values from hydrogen spectroscopy experiments. Chronological overview of the values of the proton charge radius (r_p) obtained from hydrogen spectroscopy experiments, including those taken into account in the CODATA 2014 adjustment[75] and four more recent measurements. The data points are labelled by their location and the measured transition. The wide, blue band represents the CODATA 2014 recommended value obtained from hydrogen and deuterium (H–D) spectroscopy[75], and the thin, red band corresponds to the best estimate of the CREMA Collaboration[18] using muonic hydrogen (μH) spectroscopy. The error bars represent one standard deviation. Adapted with permission from ref.[120], Wiley-VCH. Data from refs[24–26, 121–130].

improved in several respects. The measurement was performed using a specially developed technique called frequency-offset separated oscillatory fields, which is a variant of the Ramsey method of separated oscillatory fields. The time separation between the Ramsey pulses is selected based on a trade-off between high resolution (favoured by a long time separation) and sufficient signal-to-noise ratio (as atoms in the $2P_{1/2}$ state decay with a lifetime of 1.6 ns). The high statistics allowed the measurements to be repeated with different sets of operating parameters (beam speed, distance between Ramsey regions and excitation field amplitude) to check for systematics. In particular, the AC Stark shift was accurately modelled by numerically solving the density-matrix equations along the trajectory of the atoms. The same group also performed a detailed re-analysis of the earlier experiment by Lundeen and Pipkin[122], showing that the error bars were underestimated by about a factor of two[141]. After this re-evaluation, the result from Lundeen and Pipkin[122] was found to be compatible with both the large and small proton radius.

Future measurements

As of today, the agreement of the most recent scattering[27] and spectroscopy[26] experiments with the muonic hydrogen results undoubtedly represents an important, albeit not statistically significant enough, step towards the resolution of the proton-radius puzzle. It is premature to claim that this puzzle is solved as the discrepancies with earlier experiments are not yet understood. There is need for more scattering and spectroscopy measurements to confirm (or disprove) the convergence of these two experimental methods towards the small radius.

Scattering landscape

Owing to the nature of the scattering measurement of r_p, it is unlikely that a single scattering experiment will ever reach the precision of muonic atom spectroscopy: the most accurate scattering experiment is still ∼10 times worse than CREMA's. The
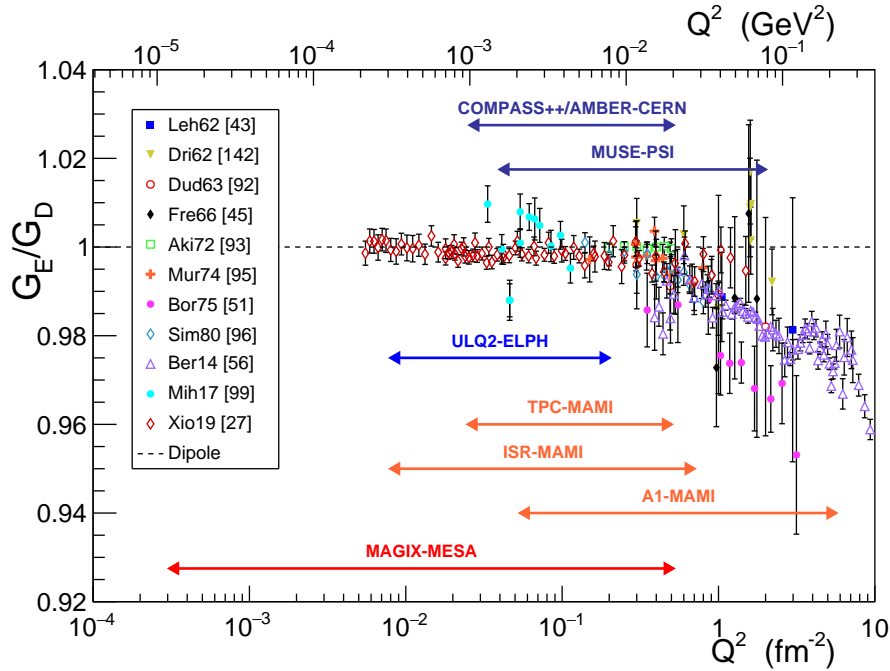
Figure 4. Measurements of the electric form factor. Past and planned measurements of the proton electric form factor (G_E) measurements at low squared four-momentum transfer (Q^2) compared with the historical dipole parameterization $G_D = \left(1 + (Q^2/0.71)\right)^{-2}$, with Q^2 in GeV^2 units. The Q^2 coverage of each experiment is indicated by a line labelled with the experiment name and location. The dipole parameterization is also shown for comparison. The error bars represent one standard deviation. Data from refs[27,43,45,51,56,92,93,95,96,99,142]. The data from ref.[56] are restricted to the Rosenbluth subset.

only reasonable direction towards the precision goal is a global analysis of combined accurate experimental data, covering a wide enough Q^2 range from the smallest possible Q^2. This is motivating the measurement of the proton electric form factor at low and very low Q^2 (Fig. 4). In this region, the small amplitude of the variation of the electric form factor and the reduced Q^2 interval of a single experiment impose severe accuracy constraints[137,143] on cross-section experiments, which must aim for systematic errors of a few tenths of a percent. This experimental challenge is being addressed using different techniques. At MAMI, the original 2010 measurement is being repeated with a hydrogen-gas jet target and an improved procedure for luminosity monitoring. The purity of the target, its point-like nature and the accurate monitoring of the relative normalization between measurements at different beam energies and spectrometer positions guarantee strict control of systematics. The results from this renewal of the 2010 experiment are particularly awaited in view of the discrepancy with the PRad measurement. The recently demonstrated initial-state radiation method[99] allows smaller Q^2 to be reached by taking advantage of the energy decrease of the electron beam after radiating a photon. This technique involves the most refined understanding of QED radiative effects up to multi-photon emission. Another technique under development at MAMI is the detection of the recoil proton in a pressured time projection chamber. The detection of protons has already proved to be accurate in r_p-related studies[93,95] but has not been attempted at such low recoil energies. At the future MESA (Mainz Energy-Recovering Superconducting Accelerator), the MAGIX[144] experiment aims to reach even smaller Q^2 by investigating the e–p reaction at lower beam energies and multiple scattering angles to perform a Rosenbluth separation using spectrometers and a point-like hydrogen target. Finally, at the Research Center for Electron Photon Science (ELPH, Japan) the ULQ2 experiment[145] aims to measure the e–p cross section relative to the e–^{12}C elastic scattering to perform a Rosenbluth separation using a pair of spectrometers.

Another perspective[146–151] is to explore the possibility that the difference between results from electron scattering and muonic atom spectroscopy is due to the manifestation of new physics beyond the Standard Model: in some way, electrons and muons would behave differently, and consequently lepton universality would be violated. Such a hypothetical possibility has also been proposed to explain the measured deviation ($>3\sigma$) of the muon magnetic moment from the Standard Model prediction[152,153]. The anomaly observed for the internal pair creation process in ^{8}Be (ref.[154]) and ^{4}He (ref.[155]) may be a further indication. The existence of a new scalar boson, also referred to as a dark photon, might explain the difference between the behaviour of muons and electrons and simultaneously resolve the proton-radius puzzle and the muon anomaly. The coupling strength of this new particle to electrons and muons is small, but the domain of low-mass particles might be accessible to

scattering experiments[156]. Whereas atomic spectroscopy provides a comparison ground for electrons and muons, no equivalent yet exists for scattering experiments. The MUSE[157] experiment at PSI fills this gap by simultaneously investigating $\mu^\pm$–p and $e^\pm$–p scattering with a non-magnetic device. This not only addresses an as yet unexplored part of the puzzle, but also tests the reliability of the Born approximation for both lepton species. Another project under development at CERN (Switzerland) within the COMPASS++/AMBER[158] experiment intends to measure $\mu^\pm$–p elastic scattering by detecting the recoil proton with a time projection chamber.

As of today, MUSE and A1-MAMI (Fig. 4) are collecting data, and the other experimental projects are expected to run within the next 5 years. These are all challenging experiments in view of the required precision, but can be reasonably expected to indisputably establish the r_p value – as determined from the scattering technique – in the near future.

Spectroscopy efforts

In view of the discrepancies between measurements of different lines in ordinary hydrogen, further spectroscopy measurements are under development to complement and improve upon previous data. The 1S–3S measurements will be further improved in both Paris[25,120] and Garching[130], with different experimental approaches involving a continuous-wave and pulsed excitation laser, respectively, providing a valuable cross-check. New transitions will also be investigated: 2S–6P in Garching[159] and 1S–4S in Paris[160]. With minor modifications, the same measurements can be repeated for deuterium to investigate the discrepancy in the deuteron radius[19]. The difficulties facing precision measurements in hydrogen also motivate the investigation of other atomic and molecular systems. Although only a few systems are directly sensitive to r_p (hydrogen molecules or molecular ions), indirect information can be obtained by determining the Rydberg constant, which is strongly correlated to r_p by the very precise measurement of the 1S–2S transition in hydrogen. It is thus interesting to study systems in which the nucleus (or nuclei) is not a proton, if they have some specific conceptual or experimental advantages for the determination of the Rydberg constant. Finally, determining the values of other nuclear radii is also of interest to check the agreement between the different experimental methods. This would allow testing of beyond the Standard Model (BSM) physics hypotheses that involve different couplings for protons and neutrons. The current status of research on the most relevant systems is summarized in Fig. 5.

Several hydrogen-like atoms may provide important new data. Positronium (Ps $\equiv e^+e^-$) and muonium (M $\equiv \mu^+e^-$) are purely leptonic systems that would allow the Rydberg constant to be determined independently of any nuclear effects and are sensitive probes of BSM physics[164]. Ongoing positronium projects in Zurich[165], Riverside (California)[166] and London[167] aim to improve the measurement of the 1S–2S transition or measure narrow transitions between the 2^3S_1 state and high-n Rydberg states, and may ultimately reach precisions in the parts-per-trillion range. The equal masses of positronium constituents make QED calculations much more complex than in hydrogen; ongoing theoretical developments (see, for example, ref.[168]) are expected to reduce the theoretical uncertainty to below 10 ppt. In muonium, an experiment to increase the precision of the measurement of the 1S–2S transition frequency is in preparation at PSI[169].

A different system is the He$^+$ ion, for which measurements of the 1S–2S transition in progress in Garching[170] and Amsterdam[171,172] could yield new values of the ^{3}He and ^{4}He nuclear radii, to be compared with results from muonic helium spectroscopy. There are both experimental and theoretical challenges, including the development of precise frequency comb spectroscopy at the deep-UV transition wavelength and the improvement of the theoretical accuracy, which is currently limited by two-loop radiative corrections[173].

Nuclear radii could also be obtained from the neutral helium atom[174], which is experimentally more convenient but theoretically more complicated than He$^+$. The doubly forbidden transition 2^3S_1–2^1S_0 in ^{4}He was recently measured[175] with an unprecedented precision of 10^{-12}. Further advances in calculations of QED corrections would allow the nuclear charge radius to be determined to better than 1%. The present state of theory already allows for comparison of differences of squared nuclear radii from isotope-shift measurements. However, different experiments on the ^{3}He–^{4}He isotope shift show significant discrepancies[174,176]. Results from muonic helium spectroscopy[177] should soon yield new insight into this problem.

Spectroscopy of the simplest molecules — the hydrogen molecular ions H$_2^+$ and HD$^+$ (ref.[178]) or neutral molecules H$_2$ and HD (ref.[179]) — has been proposed to determine the Rydberg constant as well as the proton and deuteron radii. In these molecules, the ro-vibrational transition frequencies also depend on the nuclear-to-electron mass ratios, requiring several measurements to disentangle the constants involved. In molecular ions, Doppler-free spectroscopy methods[178,184,185] have recently enabled the experimental precision to be improved to a few 10^{-12} (refs.[186,187]), overtaking the theoretical precision[188] by a factor of ~ 3. In neutral hydrogen molecules, the experimental[181–183] and theoretical[189] precisions have reached the 10^{-10} range and can be substantially improved, even though two-electron systems are theoretically more complex.

Another interesting possibility is the spectroscopy of Rydberg states in hydrogen-like ions[190] or many-electron atoms[191], exploiting the very high theoretical accuracy due to the strong suppression of QED corrections.

The completion of these projects will result in independent values of the proton radius and Rydberg constants, which will enable validation of the (electronic) hydrogen spectroscopy results and might thus provide decisive insight into the remaining discrepancies between electronic and muonic hydrogen. At the time of writing, an improved determination of helium nuclear
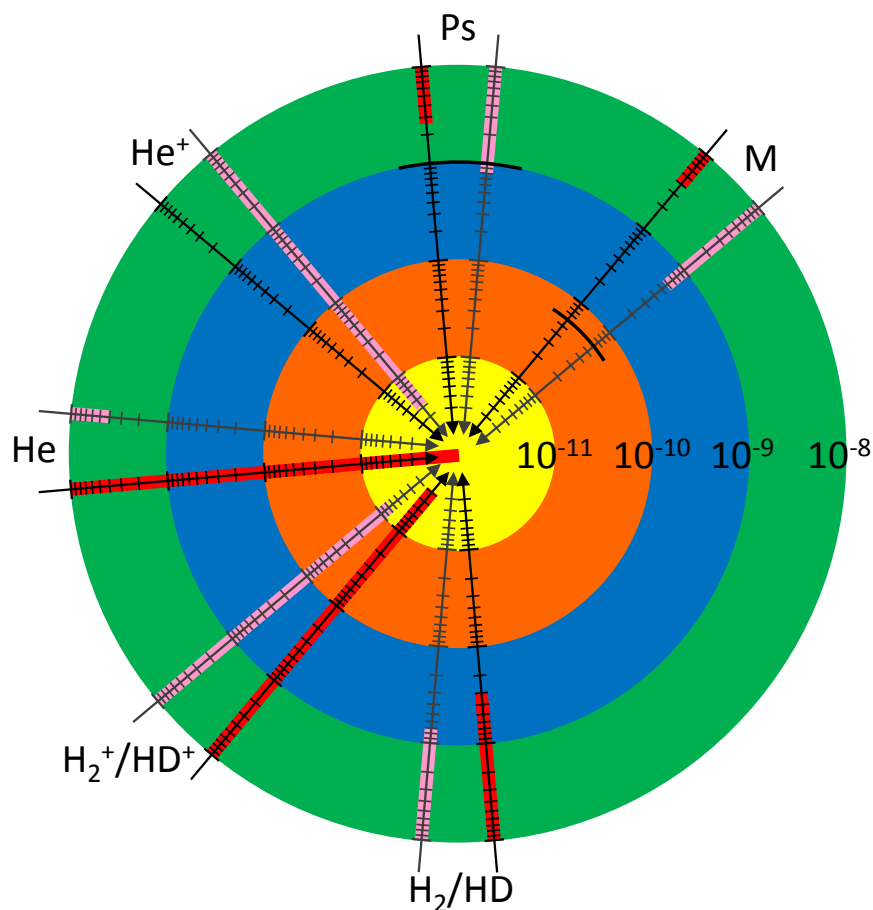
Figure 5. Precision spectroscopy of light atoms and molecules. The precision spectroscopy of light atoms and molecules could provide new data related to the proton charge radius. The red and pink bars indicate (on a logarithmic scale) the best experimental and theoretical accuracies, respectively, reported so far. The natural widths of the transitions, if larger than 1 ppt of the frequency, are indicated by black arcs. The 'archery target' representation enables convenient comparison of different systems but does not convey the idea of competing efforts, because each system is studied with different goals. For the meaningful independent determination of the Rydberg constant, which is known with a relative uncertainty of 5.9 ppt according to the 2014 CODATA analysis (or 1.9 ppt in the 2018 CODATA analysis), both the experimental and theoretical precisions should reach a few 10^{-12}, that is, get closer to the target centre. The precision data is taken for the 1S–2S transition in muonium (M)[161,162], positronium (Ps)[163,167] and He+(ref.[173]); the $2\,^3S_1$–$2\,^1S_0$ transition in He (refs[174,175]); the 0-9 vibrational overtone in HD+ (refs[187,188]); and the dissociation energy of ortho-H_2 (refs[183,189]).

radii from muonic helium spectroscopy is expected in the near future. Several additional measurements in hydrogen molecular ions at the few parts-per-trillion level, along with further progress in the theory, would enable a sub-percent determination of the proton radius.Intensive efforts are being devoted to the He+ ion and might yield, within a few years, a new value of the helium radius and a very precise test of bound-state QED calculations.

Outlook

The experimental results collected over the past 3 years are a breakthrough towards a resolution of the proton-radius puzzle. These results weaken the tension between the atomic and subatomic determinations of the proton charge radius, and hint at the possibility that the observed discrepancies are due to unknown or underestimated systematic errors in both electronic hydrogen spectroscopy and electron scattering. As more data from experiments with improved control of systematics are accumulated, both experimental methods would eventually come to agree with the highly precise muonic value. It is, however, too early to take such a scenario for granted, and further investigations are needed to pinpoint the origin of the observed deviations. Concerning scattering experiments, the upcoming results from MAMI and MUSE are particularly awaited, with the latter providing a crucial test of the lepton non-universality hypothesis. As for hydrogen spectroscopy, further measurements of the

1S–3S transition using two different approaches may allow further progress in understanding the systematics. Meanwhile, as no weakness has been found in the muonic experiments and in the related theory, CODATA logically included the muonic determination in their latest adjustment, yielding the 2018 CODATA-recommended value of $r_p = 0.8414(19)$ fm (CODATA internationally recommended 2018 values of the fundamental physical constants).

To end this Review, it is worthwhile reflecting briefly on what would be the consequences if the current trend of a small proton charge radius is confirmed by future ordinary hydrogen spectroscopy and scattering experiments. What will we have learned from the proton-radius puzzle?

Regarding spectroscopy, confirming the small proton radius would conclusively establish muonic atom laser spectroscopy as the most reliable and precise method to determine the size of light nuclei. Ongoing work of the CREMA collaboration on muonic helium, lithium and beryllium[192] can be expected to produce a wealth of new data, providing deeper insight into the internal structure of light nuclei. The impact on spectroscopy of simple atoms and molecules would also be important, as resolving the proton radius discrepancy also means confirming the value of the Rydberg constant, which reinforces the predictive power of QED calculations. The focus of other spectroscopy experiments sensitive to this constant would then shift back to their original goals, such as the determination of other atomic fundamental constants or searches for new physics.

Concerning lepton scattering, this puzzle challenges as never before the achievable data precision, pushing the limits of the reduction of experimental and theoretical systematic errors. This has motivated a new generation of experimental techniques, which benefit the nuclear physics community and beyond. In particular, the accuracy of the techniques developed in elastic electron scattering is of interest for the study of radioactive nuclei. Furthermore, the data interpolation issue has motivated the development of multivariate analysis methods that are providing new insight in the determination of the proton charge radius from experimental data. The confirmation of a small radius would then enable further investigations of the proton structure, such as its relativistic nature and higher-order spatial moments. The proton-radius puzzle has also engendered a close and fruitful collaboration between nuclear and atomic physicists, both experimentalists and theorists. This puzzle will be considered definitely solved only once all the observed discrepancies are fully understood, which would be an achievement in itself.

References

1. E. Rutherford, Phil. Mag. **21**, 669 (1911).
2. E. Rutherford, Phil. Mag. **37**, 537 (1919); 562 (1919); 571 (1919); 581 (1919).
3. R. Frisch, O. Stern, Z. Phys. **85**, 4 (1933).
4. I. Esterman, O. Stern, Z. Phys. **85**, 17 (1933).
5. R. Hofstadter, R.W. McAllister, Phys. Rev. **98**, 217 (1955).
6. M. Gell-Mann, Phys. Lett. B **8**, 214 (1964).
7. G. Zweig, CERN Report 8419/TH.412 (1964); 8182/TH.401 (1964).
8. M. Breidenbach *et al.* Phys. Rev. Lett. **23**, 935 (1969).
9. D. Müller, D. Robaschik, D. Geyer, F.M. Dittes, J. Horejši, Fortschr. Phys. **42**, 101 (1994).
10. X. Ji, Phys. Rev. Lett. **78**, 610 (1997).
11. A.V. Radyushkin, Phys. Rev. D **56**, 5524 (1997).
12. (HERMES Collaboration) A. Airapetian *et al.* Phys. Rev. Lett. **87**, 182001 (2001).
13. (CLAS Collaboration) S. Stepanyan *et al.* Phys. Rev. Lett. **87**, 182002 (2001).
14. P.J. Mohr, B.N. Taylor, D.B. Newell, Rev. Mod. Phys. **80**, 633 (2008).
15. I. Sick, Phys. Lett. B **576**, 62 (2003).
16. (A1 Collaboration) J.C. Bernauer *et al.* Phys. Rev. Lett. **105**, 242001 (2010).
17. (CREMA Collaboration) R. Pohl *et al.* Nature **466**, 213 (2010).
18. (CREMA Collaboration) A. Antognini et al. Science **339**, 417 (2013).
19. R. Pohl *et al.* Science **353**, 669 (2016).
20. R. Pohl, R. Gilman, G.A. Miller, K. Pachucki, Annu. Rev. Nucl. Part. Sci. **63**, 175 (2013).
21. J.C. Bernauer, R. Pohl, Sci. Am. **310**, 32 (2014).
22. C.E. Carlson, Prog. Part. Nucl. Phys.**82**, 59 (2015).
23. R.J. Hill, EPJ Web Conf. **137**, 01023 (2017).

24. A. Beyer *et al.* Science **358**, 79 (2017).

25. H. Fleurbaey *et al.* Phys. Rev. Lett. **120**, 183001 (2018).

26. N. Bezginov, T. Valdez, M. Horbatsch, A. Marsman, A.C. Vutha, E. A. Hessels, Science **365**, 1007 (2019).

27. (PRad Collaboration) W. Xiong *et al.* Nature **575**, 147 (2019).

28. M.N. Rosenbluth, Phys. Rev. **79**, 615 (1950).

29. V. Punjabi, C.F. Perdrisat, M.K. Jones, E.J. Brash, C.E. Carlson, Eur. Phys. J. A **51**, 79 (2015).

30. A.I. Akhiezer, M.P. Rekalo, Sov. Phys. Dokl. **13**, 572 (1968).

31. A.I. Akhiezer, M.P. Rekalo, Sov. J. Part. Nucl. Phys. **4**, 277 (1974).

32. R.G. Arnold, C.E. Carlson, F. Gross, Phys. Rev. C **23**, 363 (1981).

33. N. Dombey, Rev. Mod. Phys. **41**, 236 (1969).

34. P.A.M. Guichon, M. Vanderhaeghen, Phys. Rev. Lett. **91**, 142303 (2003).

35. P.G. Blunden, W. Melnitchouk, J.A. Tjon, Phys. Rev. Lett. **91**, 142304 (2003).

36. (CLAS Collaboration) D. Adikaram *et al.* Phys. Rev. Lett. **114**, 062003 (2015).

37. I.A. Rachek *et al.* Phys. Rev. Lett. **114**, 062005 (2015).

38. (OLYMPUS Collaboration) B.S. Henderson *et al.* Phys. Rev. Lett. **118**, 092501 (2017).

39. M. Gorchtein, Phys. Rev. C **90**, 052201 (2014).

40. O. Tomalak, B. Pasquini, M. Vanderhaeghen, Phys. Rev. D **96**, 096001 (2017).

41. G. Miller, Phys. Rev. C **99**, 035202 (2019).

42. F. Bumiller, M. Croissiaux, E. Dally, R. Hofstadter, Phys. Rev. **124**, 1623 (1961)

43. P. Lehmann, R. Taylor, R. Wilson, Phys. Rev. **126**, 1183 (1962).

44. K.W. Chen, J.R. Dunning, Jr., A.A. Cone, N.F. Ramsey, J.K. Walker, R. Wilson, Phys. Rev. **141**, 1267 (1966).

45. D. Frèrejacque, D. Benaksas, D. Drickey, Phys. Rev. **141**, 1308 (1966).

46. W. Bartel *et al.* Nucl. Phys. B **58**, 608 (1966).

47. T. Janssens, R. Hofstadter, E.B. Hughes, M.R. Yearian, Phys. Rev. **124**, 922 (1966).

48. Ch. Berger, V. Burkert, G. Knop, B. Langenbech, K. Rith, Phys. Lett. B **35**, 87 (1971).

49. L.E. Price, J.R. Dunning, Jr., M. Goitein, K. Hanson, T. Kirk, R. Wilson, Phys. Rev. D **4**, 45 (1971).

50. W. Bartel *et al.* Phys. Rev. Lett. **17**, 429 (1973).

51. F. Borkowski, G.G. Simon, V.H. Walther, R.D. Wendling, Nucl. Phys. B **93**, 461 (1975).

52. R.C. Walker *et al.* Phys. Rev. D **49**, 5671 (1994).

53. L. Andivahis *et al.* Phys. Rev. D **50**, 5491 (1994).

54. M.E. Christy *et al.* Phys. Rev. C **70**, 015206 (2004).

55. I.A. Qattan *et al.* Phys. Rev. Lett. **94**, 142301 (2005).

56. (A1 Collaboration) J.C. Bernauer *et al.* Phys. Rev. C **90**, 015206 (2014).

57. (Bates FPP Collaboration) B.D. Milbrath *et al.* Phys. Rev. Lett. **80**, 452 (1998).

58. S. Dieterich *et al.* Phys. Lett. B **500**, 47 (2001).

59. (The Jefferson Lab Hall A Collaboration) 0. Gayou *et al.* Phys. Rev. C **64**, 038202 (2001).

60. Th. Pospischil *et al.* Eur. Phys J. A **12**, 125 (2001).

61. S. Strauch *et al.* Phys. Rev. Lett. **91**, 052301 (2003).

62. (The Jefferson Lab Hall A Collaboration) V. Punjabi *et al.* Phys. Rev. C **71**, 055202 (2005).

63. G. MacLachlan *et al.* Nucl. Phys. A **764**, 261 (2006).

64. (Resonance Spin Structure Collaboration) M.K. Jones *et al.* Phys. Rev. C **74**, 035201 (2006).

65. C.B. Crawford *et al.* Phys. Rev. Lett. **98**, 052301 (2007).

66. (E03-104 Collaboration) M. Paolone *et al.* Phys. Rev. Lett. **105**, 072001 (2010).

67. (GEp2γ Collaboration) M. Meziane *et al.* Phys. Rev. Lett. **106**, 132501 (2011).

68. X. Zhan *et al.* Phys. Lett. B **705**, 59 (2011).

69. (The Jefferson Lab Hall A Collaboration) G. Ron *et al.* Phys. Rev. C **84**, 055204 (2011).

70. (The Jefferson Lab Hall A Collaboration) A.J.R. Puckett *et al.* Phys. Rev. C **85**, 045203 (2012).

71. A.J.R. Puckett *et al.* Phys. Rev. C **96**, 055203 (2017); Phys. Rev. C **98**, 019907(E) (2018).

72. R. Karplus, A. Klein, J. Schwinger, Phys. Rev. **86**, 288 (1952).

73. W.E. Lamb, R.C. Retherford, Phys. Rev. **72**, 241 (1947).

74. M.I. Eides, H. Grotch, V.A. Shelyuto, Phys. Rep. **342**, 63 (2001).

75. P.J. Mohr, D.B. Newell, B.N. Taylor, Rev. Mod. Phys. **88**, 035009 (2016).

76. C.G. Parthey *et al.* Phys. Rev. Lett. **107**, 203001 (2011).

77. A. Matveev *et al.* Phys. Rev. Lett. **110**, 230801 (2013).

78. A. Antognini, F. Kottmann, F. Biraben, P. Indelicato, F. Nez, R. Pohl, Ann. Phys. **331**, 127 (2013).

79. K. Pachucki, Phys. Rev. A **53**, 2092 (1996).

80. K. Pachucki, Phys. Rev. A **60**, 3593 (1999).

81. S.G. Karshenboim, E.Yu. Korzinin, V.G. Ivanov, V.A. Shelyuto, JETP Lett. **92**, 8 (2010).

82. U.D. Jentschura, Ann. Phys. **326**, 500 (2011).

83. U.D. Jentschura, Phys. Rev. A **84**, 012505 (2011).

84. E. Borie, Ann. Phys. **327**, 733 (2012).

85. S.G. Karshenboim, V.G. Ivanov, E.Yu. Korzinin, Phys. Rev. A **85**, 032509 (2012).

86. P. Indelicato, Phys. Rev. A **87**, 022501 (2013).

87. K. Pachucki, V. Patkos, V. Yerokhin, Phys. Rev. A **97**, 062511 (2018).

88. G.A. Miller, Phys. Lett. B **718**, 1078 (2012).

89. M.C. Birse, J.A. McGovern, Eur. Phys. J. A **48**, 120 (2012).

90. J.M. Alarcón, V. Lensky, V. Pascalutsa, Eur. Phys. J. C **74**, 2852 (2014).

91. E.E. Chambers, R. Hofstadter, Phys. Rev. **103**, 1454 (1956).

92. B. Dudelzak, G. Sauvage, P. Lehmann, Il Nuovo Cim. **28**, 18 (1963).

93. Yu.K. Akimov *et al.* Sov. Phys. JETP **35**, 651 (1972).

94. F. Borkowski, P. Peuser, G.G. Simon, V.H. Walther, R.D. Wendling, Nucl. Phys. A **222**, 269 (1974).

95. J.J. Murphy, II, Y.M. Shin, D.M. Skopik, Phys. Rev. C **9**, 2125 (1974).

96. G.G. Simon, Ch. Schmitt, F. Borkowski, V.H. Walther, Nucl. Phys. A **333**, 381 (1980).

97. M. McCord, H. Crannell, L.W. Fagg, J.T. O'Brien, D.I. Sober, J.W. Lightbody, X.K. Maruyama, P.A. Treado, Nucl. Inst. Meth. B **56-57**, 496 (1991).

98. (SELEX Collaboration) M. Eschrich *et al.* Phys. Lett. B **522**, 233 (2001).

99. (A1 Collaboration) M. Mihovilovič *et al.* Phys. Lett. B **771**, 194 (2017); arXiv:1905.1182, (2019).

100. L.N. Hand, D.G. Miller, R. Wilson, Rev. Mod. Phys. **35**, 335 (1963).

101. G. Höhler, E. Pietarinen, I. Sabba-Stefanescu, F. Borkowski, G.G. Simon, V.H. Walther, R.D. Wendling, Nucl. Phys. B **114**, 505 (1976).

102. P. Mergell, Ulf-G. Meißner, D. Drechsel, Nucl.Phys. A **596**, 367 (1996).

103. R. Rosenfelder, Phys. Lett. B **479**, 381 (2000).

104. P.G. Blunden, I. Sick, Phys. Rev. C **72**, 057601 (2005).

105. M.A. Belushkin, H.-W. Hammer, Ulf-G. Meißner, Phys. Rev. C **75**, 035202 (2007).

106. D. Borisyuk, Nucl. Phys. A **843**, 59 (2010).

107. R.J. Hill, G. Paz, Phys. Rev. D **82**, 113005 (2010).

108. I. Sick, Prog. Part. Nucl. Phys. **67**, 473 (2012).

109. C. Adamuscin, S. Dubnicka, A.Z. Dubnickova, Prog. Part. Nucl. Phys. **67**, 479 (2012).

110. L.T. Lorenz, H.-W. Hammer, Ulf-G. Meißner, Eur. Phys. J. A **48**, 151 (2012).

111. K.M. Graczyk, C. Juszczak, Phys. Rev. C **90**, 054334 (2014).

112. I.T. Lorenz, Ulf-G. Meißner, H.-W. Hammer, Y.-B. Dong, Phys. Rev. D **91** (2015) 014023.

113. J. Arrington, I. Sick, J. Phys. Chem. Ref. Data **44**, 031204 (2015).

114. G. Lee, J. Arrington, R. Hill, Phys. Rev. D **92**, 013013 (2015).

115. D.W. Higinbotham, Al.A. Kamin, V. Lin, D. Meekins, B. Norum, B. Sawatzky, Phys. Rev. C **93**, 055207 (2016).

116. K. Griffioen, C. Carlson, S. Maddox, Phys. Rev. C **93**, 065207 (2016).

117. M. Horbatsch, E. Hessels, Phys. Rev. C **95**, 035203 (2017).

118. I. Sick, Atoms **6**, 2 (2018).

119. J.M. Alarcón, D.W. Higinbotham, C. Weiss, Z. Ye, arXiv:1809.06373 (2018).

120. S. Thomas, H. Fleurbaey, S. Galtier, L. Julien, F. Biraben, F. Nez, Ann. Phys. **531**, 1800363 (2019).

121. G.F. Newton, D.A. Andrews, P.J. Unsworth, Phil. Trans. R. Soc. A **290**, 373 (1979).

122. S.R. Lundeen, F.M. Pipkin, Metrologia **22**, 9 (1986).

123. E.W. Hagley, F.M. Pipkin, Phys. Rev. Lett. **72**, 1172 (1994).

124. D.J. Berkeland, E.A. Hinds, M.G. Boshier, Phys. Rev. Lett. **75**, 2470 (1995).

125. M. Weitz, A. Huber, F. Schmidt-Kaler, D. Leibfried, W. Vassen, C. Zimmermann, K. Pachucki, T.W. Hänsch, L. Julien, F. Biraben, Phys. Rev. A **52**, 2664 (1995).

126. S. Bourzeix, B. de Beauvoir, F. Nez, M.D. Plimmer, F. de Tomasi, L. Julien, F. Biraben, D.N. Stacey, Phys. Rev. Lett. **76**, 384 (1996).

127. B. de Beauvoir, F. Nez, L. Julien, B. Cagnac, F. Biraben, D. Touahri, L. Hilico, O. Acef, A. Clairon, J.J. Zondy, Phys. Rev. Lett. **78**, 440 (1997).

128. C. Schwob, L. Jozefowski, B. de Beauvoir, L. Hilico, F. Nez, L. Julien, F. Biraben, O. Acef, A. Clairon, Phys. Rev. Lett. **82**, 4960 (1999); **86**, 4193(E) (2001).

129. O. Arnoult, F. Nez, L. Julien, F. Biraben, Eur. Phys. J. D **60**, 243 (2010).

130. D.C. Yost, A. Matveev, A. Grinin, E. Peters, L. Maisenbacher, A. Beyer, R. Pohl, N. Kolachevsky, K. Khabarova, T.W. Hänsch, Th. Udem, Phys. Rev. A **93**, 042509 (2016).

131. R. Hill, Phys. Rev. D **95**, 013001 (2017).

132. S.K. Barcus, D. Higinbotham, R.E. McClellan, arXiv:1902.08185 (2019).

133. E. Kraus, K.E. Mesick, A. White, R. Gilman, S. Strauch, Phys. Rev. C **90**, 045206 (2014).

134. X. Yan, D.W. Higinbotham, D. Dutta, H. Gao, A. Gasparian, M.A. Khandaker, N. Liyanage, E. Pasyuk, C. Peng, W. Xiong, Phys. Rev. **98**, 025204 (2018).

135. I. Lorenz, U.G.-Meißner, Phys. Lett. B **737**, 57 (2014).

136. M. Horbatsch, E.A. Hessels, Phys. Rev. C **93**, 015204 (2016).

137. I. Sick, D. Trautmann, Phys. Rev. C **95**, 012501 (2017).

138. V. Yerokhin, K. Pachucki, V. Patkós, Ann. Phys. **531**, 1800324 (2019).

139. S.G. Karshenboim, V.A. Shelyuto, Phys. Rev. A **100**, 032513 (2019).

140. S.G. Karshenboim, A. Ozawa, V.G. Ivanov, Phys. Rev. A **100**, 032515 (2019).

141. A. Marsman, M. Horbatsch, Z.A. Corriveau, E.A. Hessels, Phys. Rev. A **98**, 012509 (2018).

142. D.J. Drickey, L.N. Hand, Phys. Rev. Lett. **9** (1962) 521.

143. M. Hoballah *et al.* Eur. Phys. J. A **55**, 112 (2019).

144. H. Merkel, PoS (BORMIO 2016), 037 (2016).

145. T. Suda *et al.* J. Part. Acc. Soc. Japan **15**, 52 (2018).

146. V. Barger, C.W. Chiang, W.Y. Keung, D. Marfatia, Phys. Rev. Lett. **106**, 153001 (2011).

147. D. Tucker-Smith, I. Yavin, Phys. Rev. D **83**, 101702 (2011).

148. B. Batell, D. McKeen, M. Pospelov, Phys. Rev. Lett. **107**, 011803 (2011).

149. C.E. Carlson, B.C. Rislow, Phys. Rev. D **86**, 035013 (2012).

150. V. Pauk, M. Vanderhaeghen, Phys. Rev. Lett. **115**, 221804 (2015).

151. Yu-S. Liu, G.A. Miller, Phys. Rev. C **92**, 035209 (2015).

152. (Muon g-2 Collaboration) G.W. Bennett *et al.* Phys. Rev. D **73**, 072003 (2006).

153. F. Jegerlehner, A. Nyffeler, Phys. Rep. **477**, 1 (2009).

154. A.J. Krasznahorkay *et al.* Phys. Rev. Lett. **116**, 042501 (2016).

155. A.J. Krasznahorkay *et al.* arXiv:1910.10459 (2019).

156. Yu-S. Liu, D. McKeen, G.A. Miller, Phys. Rev. Lett. **117**, 101801 (2016).

157. (MUon Scattering Experiment Collaboration) R. Gilman, E.J. Downie, G. Ron, S. Strauch *et al.* arXiv:1709.09753, (2017).

158. B. Adams *et al.* arXiv:1808.00848, (2018); CERN-SPSC-2019-022, (2019).

159. A. Beyer, L. Maisenbacher, K. Khabarova, A. Matveev, R. Pohl, T. Udem, T. Hänsch, N. Kolachevsky, Phys. Script.T **65**, 014030 (2015).

160. S. Galtier, F. Nez, L. Julien, F. Biraben, Opt. Comm. **324**, 34 (2014).

161. V. Meyer *et al.* Phys. Rev. Lett. **84**, 1136 (2000).

162. K.P. Jungmann in *The Hydrogen Atom*, eds. S.G. Karshenboim, F.S. Pavone, F. Bassani, M. Inguscio, T.W. Hänsch, Lect. Notes in Phys. **570** (Springer, Berlin, 2001).

163. M.S. Fee, A.P. Mills Jr., S. Chu, E.D. Shaw, K. Danzmann, R.J. Chichester, D.M. Zuckerman, Phys. Rev. Lett. **70**, 1397 (1993).

164. S.G. Karshenboim, Phys. Rep. **422**, 1 (2005).

165. D.A. Cooke et al., Hyperfine Int. **233**, 67 (2015).

166. A.P. Mills Jr., Adv. At. Mol. Opt. Phys. **65**, 265 (2016).

167. D.B. Cassidy, Eur. Phys. J. D **72**, 53 (2018).

168. G.S. Adkins, M. Kim, C. Parsons, R.N. Fell, Phys. Rev. Lett. **115**, 233401 (2015).

169. P. Crivelli, G. Wichmann, arXiv:1607.06398.

170. M. Herrmann *et al.* Phys. Rev. A **79**, 052505 (2009).

171. K. Altmann, S. Galtier, L.S. Dreissen, K.S.E. Eikema, Phys. Rev. Lett. **117**, 173201 (2016).

172. J.J. Krauth, L.S. Dreissen, C. Roth, E.L. Gründemann, M. Collombon, M. Favier, K.S.E. Eikem, PoS(FFK2019)049.

173. S.G. Karshenboim, A. Ozawa, V.A. Shelyuto, R. Szafron, V.G. Ivanov, Phys. Lett. B **795**, 432 (2019).

174. K. Pachucki, V. Patkos, V.A. Yerokhin, Phys. Rev. A **95**, 062510 (2017).

175. R.J. Rengelink, Y. van der Werf, R.P.M.J.W. Notermans, R. Jannin, K.S.E. Eikema, M.D. Hoogerland, W. Vassen, Nat. Phys. **14**, 1132 (2018).

176. X. Zheng, Y.R. Sun, J.-J. Chen, W. Jiang, K. Pachucki, S.-M. Hu, Phys. Rev. Lett. **119**, 263002 (2017).

177. B. Franke, J.J. Krauth, A. Antognini, M. Diepold, F. Kottmann, R. Pohl, Eur. Phys. J. D **71**, 341 (2017).

178. J.-Ph. Karr, L. Hilico, J.C.J. Koelemeij, V.I. Korobov, Phys. Rev. A **94**, 050501(R) (2016).

179. M. Puchalski, J. Komasa, P. Czachorowski, K. Pachucki, Phys. Rev. Lett. **117**, 263002 (2016).

180. S. Alighanbari, M.G. Hansen, V.I. Korobov, S. Schiller, Nat. Phys. **14**, 555 (2018).

181. L.-G. Tao, A.-W. Liu, K. Pachucki, J. Komasa, Y.-R. Sun, J. Wang, S.-M. Hu, Phys. Rev. Lett. **120**, 153001 (2018).

182. F.M.J. Cozijn, P. Dupre, E.J. Salumbides, K.S.E. Eikema, W. Ubachs, Phys. Rev. Lett. **120**, 153002 (2018).

183. N. Hölsch, M. Beyer, E.J. Salumbides, K.S.E. Eikela, W. Ubachs, Ch. Jungen, F. Merkt, Phys. Rev. Lett. **122**, 103002 (2019).

184. L. Hilico, N. Billy, B. Grémaud, D. Delande, J. Phys. B **34**, 491 (2001).

185. V.Q. Tran, J.-Ph. Karr, A. Douillet, J.C.J. Koelemeij, L. Hilico, Phys. Rev. A **88**, 033421 (2013).

186. S. Alighanbari, G.S. Giri, F.L. Constantin, V.I. Korobov, S. Schiller, Nature **581**, 152 (2020).

187. S. Patra et al., Science **369**, 1238 (2020).

188. V.I. Korobov, L. Hilico, J.-Ph. Karr, Phys. Rev. Lett. **118**, 233001 (2017).

189. M. Puchalski, J. Komasa, P. Czachorowski, K. Pachucki, Phys. Rev. Lett. **122**, 103003 (2019).

190. U.D. Jentschura, P.J. Mohr, J.N. Tan, B.J. Wundt, Phys. Rev. Lett. **100**, 160404 (2008).

191. A. Ramos, K. Moore, G. Raithel, Phys. Rev A **96**, 032513 (2017).

192. S. Schmidt *et al.* J. Phys. Conf. Ser. **1138**, 012010 (2018).

Acknowledgements